Research Paper

Nitric oxide-releasing prodrug triggers cancer cell death through deregulation of cellular redox balance ☆

Anna E. Maciag [a,*], Ryan J. Holland [b], Y.-S. Robert Cheng [c], Luis G. Rodriguez [d], Joseph E. Saavedra [a], Lucy M. Anderson [b], Larry K. Keefer [b]

[a] Basic Science Program, SAIC-Frederick, Inc., Frederick National Laboratory for Cancer Research, Frederick, MD, USA
[b] Chemical Biology Laboratory, Frederick National Laboratory for Cancer Research, Frederick, MD, USA
[c] Radiation Biology Branch, Center for Cancer Research, National Cancer Institute, Bethesda, MD, USA
[d] Laboratory of Proteomics and Analytical Technologies, Advanced Technology Program, SAIC-Frederick, Inc., Frederick National Laboratory for Cancer Research, Frederick, MD, USA

ARTICLE INFO

ABSTRACT

JS-K is a nitric oxide (NO)-releasing prodrug of the O^2-arylated diazeniumdiolate family that has demonstrated pronounced cytotoxicity and antitumor properties in a variety of cancer models both *in vitro* and *in vivo*. The current study of the metabolic actions of JS-K was undertaken to investigate mechanisms of its cytotoxicity. Consistent with model chemical reactions, the activating step in the metabolism of JS-K in the cell is the dearylation of the diazeniumdiolate by glutathione (GSH) via a nucleophilic aromatic substitution reaction. The resulting product (CEP/NO anion) spontaneously hydrolyzes, releasing two equivalents of NO. The GSH/GSSG redox couple is considered to be the major redox buffer of the cell, helping maintain a reducing environment under basal conditions. We have quantified the effects of JS-K on cellular GSH content, and show that JS-K markedly depletes GSH, due to JS-K's rapid uptake and cascading release of NO and reactive nitrogen species. The depletion of GSH results in alterations in the redox potential of the cellular environment, initiating MAPK stress signaling pathways, and inducing apoptosis. Microarray analysis confirmed signaling gene changes at the transcriptional level and revealed alteration in the expression of several genes crucial for maintenance of cellular redox homeostasis, as well as cell proliferation and survival, including *MYC*. Pre-treating cells with the known GSH precursor and nucleophilic reducing agent *N*-acetylcysteine prevented the signaling events that lead to apoptosis. These data indicate that multiplicative depletion of the reduced glutathione pool and deregulation of intracellular redox balance are important initial steps in the mechanism of JS-K's cytotoxic action.

© 2013 The Authors. Published by Elsevier B.V. All rights reserved.

Introduction

Diazeniumdiolate-based NO-releasing prodrugs are a growing class of promising cancer therapeutics. O^2-Arylated diazeniumdiolates release NO upon nucleophilic aromatic substitution reaction with glutathione (GSH). O^2-(2,4-Dinitrophenyl) 1-[(4-ethoxycarbonyl)piperazin-1-yl]diazen-1-ium-1,2-diolate (JS-K) (structure shown in Fig. 1) has proven effective for inhibiting growth of cancer cells in several *in vitro* and *in vivo* models [26,27,22,15,17,31]. JS-K is highly cytotoxic to leukemia and multiple myeloma cell lines and patient-derived multiple myeloma cells, with IC_{50} values ranging from 0.2 to 1.2 μM [26,27,15]. Mouse models of leukemia or multiple myeloma confirmed the effectiveness of JS-K against these blood cancers *in vivo*. The prodrug inhibited tumor growth and prolonged survival in a multiple myeloma xenograft model [15]. Importantly, JS-K was very effective against multiple myeloma cells resistant to conventional therapy with dexamethasone, doxyrubicin or
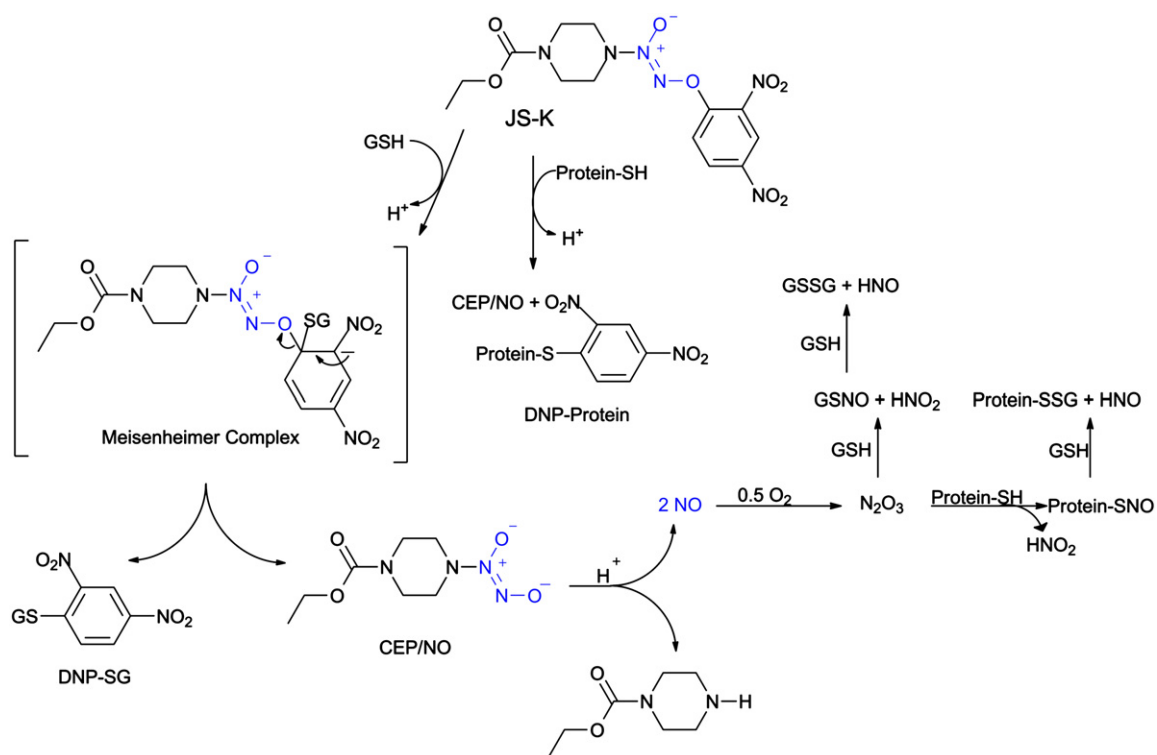
Fig. 1. Structure of JS-K and mechanism of its activation. The prodrug is activated via nucleophilic aromatic substitution, resulting in generation of NO and its oxidation products followed by a selection of subsequent reactions leading to decreases in cellular GSH/GSSG ratios.
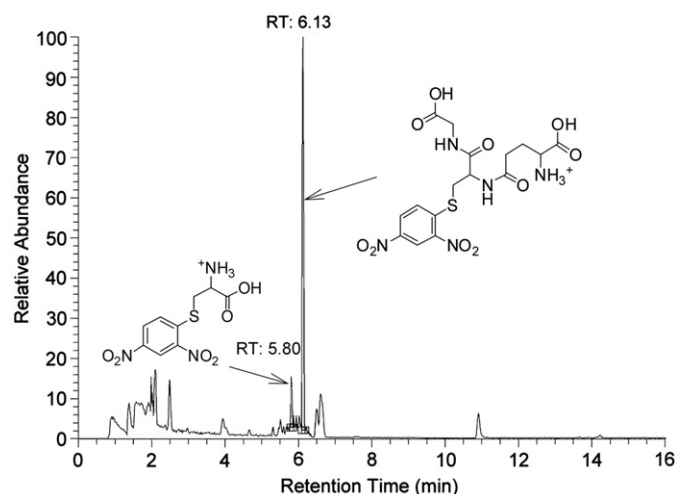

Fig. 2. GSH-dependent dearylation is a major metabolic pathway of JS-K in the cell. U937 cells were treated with 5 μM JS-K for 30 min and drug metabolites in the cell lysate were analyzed by LC/MS. The total ion current chromatogram is shown. The peak at 6.13 min is DNP-SG, while that at 5.80 min corresponds to S-(2,4-dinitrophenylated) cysteine. RT=retention time.

melphalan, with IC$_{50}$ values for these cell lines of 0.3 to 0.9 μM. Furthermore, JS-K appeared to be selectively cytotoxic towards cancer cells; no significant toxicity of the drug was observed in bone marrow stromal cells isolated from patients, at concentrations at which it inhibited the proliferation of multiple myeloma cells [15]. Similar selective toxicity towards cancer cells relative to their nonmalignant counterparts was observed in breast [18] and renal cancers [5].

The glutathione (GSH)/glutathione disulfide (GSSG) redox couple plays a central role in cellular protection against genotoxic agents and oxidants, as well as in the control of the thiol/disulfide redox state, which is essential for redox signaling [12]. GSH is the most abundant cellular antioxidant and is also involved in the detoxification of numerous xenobiotics.

Evidence from many studies suggests that cancer cells are under increased oxidative stress that is associated with oncogenic transformation. Oncogene activation or tumor suppressor inactivation in cancers commonly results in increased generation of reactive oxygen species (ROS) [24,11,20]. Leukemia cells freshly isolated from blood of chronic lymphocytic leukemia or hairy-cell leukemia patients showed increased ROS compared to normal lymphocytes [33,14]. This biochemical property of cancer cells can be exploited for therapeutic benefits. Induction of oxidative stress may be a promising approach for cancer therapy, because cancer cells with increased oxidative stress are likely to be more vulnerable to damage by additional ROS elicited by exogenous agents. NO is a relatively stable free radical that does not readily react with most macromolecules in cells. However, it reacts with oxygen and superoxide, forming reactive nitrogen species (RNS) that are highly damaging to cells.

In this study we present evidence that treatment of human leukemia U937 cells with the NO-releasing prodrug JS-K led to the depletion of GSH, affecting cellular redox potential and triggering MAPK stress signaling and apoptosis. To characterize further the biologic potential of JS-K we performed gene expression analysis using the Affymetrix platform for microarray analysis. This revealed marked alteration in expression of several genes crucial for maintenance of cellular redox homeostasis, as well as cell proliferation and survival.

Methods

JS-K synthesis, chemicals and cell culture

JS-K was synthesized as described previously [23]. All other chemicals were obtained from Sigma (St. Louis, MO). Leukemia cell line U937 [29] was obtained from the American Type Culture

Collection (Manassas, VA) and cultured in RPMI 1640 medium supplemented with 10% fetal bovine serum (FBS), glutamine and penicillin–streptomycin, at 5% CO_2, 37° C.

In vitro metabolism of JS-K

Human leukemia U937 cells were seeded in 75-cm² flasks and incubated overnight at 37° C, 5% CO_2. The cells were treated with 5 µM JS-K and incubated for 10 or 30 min. After treatment, cells were collected by centrifugation at 800g for 10 min, washed with phosphate buffered saline (PBS) and collected again. The pellets were resuspended in 800 µL of 10 mM HCl, then lysed by successive rounds of freezing and thawing. To the lysate was added 200 µL of a 5% 5-sulfosalicylic acid solution. The precipitate was removed by centrifugation at 8000g for 10 min, and the supernatant was analyzed by LC/MS using a Thermoquest Surveyor HPLC coupled with a Finnigan LCQ Deca mass spectrometer. Positive ions were generated with an atmospheric pressure chemical ionization (APCI) source with a capillary voltage of 15 V and a corona discharge of 4 µA. Separations were performed on an Agilent Eclipse XDB-C18 5-µm 4.6 × 150 mm² column at a flow rate of 1 mL/min, under H_2O/acetonitrile/0.1% formic acid gradient conditions. The stability of JS-K in a complete culture medium (RPMI 1640, 10% FBS) was determined with analogical extraction and HPLC methods.

Measurement of cellular glutathione content and cellular reduction potential

U937 cells were cultured at 1×10^6 per mL. Cells were treated in culture medium with 1 µM JS-K for 1 h or for the time periods indicated in Fig. 3. After treatment, cells were collected by centrifugation at 800g for 10 min, washed with phosphate buffered saline and collected again. The pellets were resuspended in 80 µL of 10 mM HCl and lysed by two successive rounds of freezing and thawing. Twenty microliters of a 5% 5-sulfosalicylic acid solution were added to the lysate. The precipitate was removed by centrifugation at 8000g for 10 min, and the super-natant was analyzed for total GSH content by using a total glutathione quantification kit (Dojindo, Rockville, MD) according to the manufacturer's protocol. To measure glutathione disulfide (GSSG) concentration, cells were treated and lysed in accordance with the procedure above. The lysate was then neutralized with
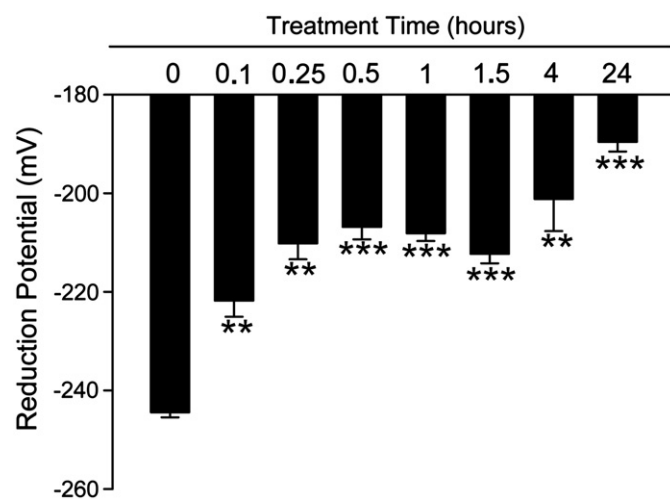
0.1 M NaOH and treated with 4-vinylpyridine at a final concentration of 50 mM for 30 min, followed by 5,5′-dithio-bis(2-nitro-benzoic acid) assay [9,1]. The results gave the total amounts of GSH and GSSG present in the cells.

To determine the intracellular concentrations of GSH and GSSG we first measured U937 cell volume. As these cells are spherical, the diameter of the cell was measured with a confocal microscope using the built-in measuring tool within the Olympus Fluoview software. Cells were stained with CellMask™ Orange plasma membrane stain at a concentration of 5 µg/mL, following the manufacturer's protocol (Invitrogen (Molecular Probes), Carlsbad, CA). Images were acquired on an Olympus FluoView 1000 confocal microscope system with a 40X objective and an excitation wavelength of 568 nm and emission wavelength of 572 nm. The average diameter of U937 cells was 19.68 ± 0.82 µm with an average radius of 9.84 ± 0.41 µm. The volume of this average sphere was calculated using the equation $V = (4/3)\pi r^3$, and resulted in an average cell volume of 4.0 ± 0.5 pL. Molar concentrations of GSH and GSSG per cell were calculated; then the reduction potential of the GSH redox couple was calculated using the equation $E_{7.4} = (E^{\circ} - (RT/nF)\log([GSH]^2/[GSSG])) + ((pH - 7.0)(\Delta E/\Delta pH))$, where E° is the electromotive force at standard conditions, R is the ideal gas constant, T is temperature in Kelvin, n is the number of electrons transferred in the redox couple ($2e^-$), F is Faraday's constant, and $(\Delta E/\Delta pH)$ is the change in reduction potential resulting from a given change in pH at 37° C.

Measurement of mitochondrial membrane potential

U937 cells were seeded on 24-well plates at 2×10^5/well and allowed to grow for 24 h. The cells were then treated in culture medium with either vehicle (DMSO) or 1–10 µM JS-K and incubated at 37 °C, 5% CO_2 for 30 min. The JC-1 Mitochondrial Membrane Potential Assay Kit (Cayman Chemical, Ann Arbor, MI) was used according to the manufacturer's protocol.

Determination of intracellular reactive oxygen/nitrogen species and nitric oxide

The intracellular levels of reactive oxygen and nitrogen species were monitored by the oxidation of the fluorophore 5-(and6)-chloromethyl-2′,7′-dichlorodihydrofluorescein diacetate (DCFH-DA) (Invitrogen). U937 cells were incubated with 5 µM DCF-DA in Hank's balanced salt solution (HBSS) at 37 °C and 5% CO_2 for 30 min. The cells were collected by centrifugation, the HBSS containing the probe was removed, and the cells were rinsed with HBSS and resuspended in fresh HBSS. Three mL of cell suspension was aliquoted into 15-mL test tubes followed by addition of JS-K or DMSO as a control. After 60 min of incubation at 37° C, 2′,7′-dichlorofluorescein (DCF) fluorescence was measured by using a PerkinElmer Life and Analytical Sciences (Waltham, MA) LS50B luminescence spectrometer with the excitation source at 488 nm and emission at 530 nm.

The intracellular level of nitric oxide after JS-K treatment was estimated using the NO-sensitive fluorophore 4-amino-5-methy-lamino-2′,7′-difluorofluorescein (DAF-FM) diacetate (Invitrogen). This reagent hydrolyzes after being taken up by the cell, where it reacts with nitrosating agents formed upon 1-electron oxidation of NO to generate a fluorescent species whose intensity is taken as a measure of intracellular NO. Cells were loaded with 2.5 µM DAF-FM diacetate in HBSS at 37 °C and 5% CO_2. After 30 min of incubation the cells were rinsed with HBSS to remove excess probe, resuspended in fresh HBSS, and treated with JS-K at 1 µM final concentration. After 60-min incubation the fluorescence of the benzotriazole derivative formed on DAF-FM's reaction with aerobic NO was analyzed by using a PerkinElmer Life and

Fig. 3. Time course of changes in cellular reduction potential after treating U937 cells with 1 µM JS-K. ***$P < 0.0001$ and **$P < 0.001$.

Analytical Sciences LS50B luminescence spectrometer with the excitation source at 495 nm and emission at 515 nm.

Immunoblotting

Western blot analysis was performed as previously described [17]. Primary antibodies for phospho-p38, p38, phospho-SAPK/JNK, SAPK/JNK, phospho-ATF2, phospho-c-jun, c-jun, caspases 3, 7, and 8, cytochrome c, PARP and cleaved PARP, c-myc (Cell Signaling Technology, Danvers, MA) and ATF3 (Santa Cruz Biotechnology, Santa Cruz, CA) were used.

Microarray analysis

RNA extraction and transcriptome profiling. Total RNAs from three independent cultures for each treatment time point or control were extracted using TRIzol reagent (Invitrogen) following the manufacturer's protocol. RNA qualities were checked by the 260 nm/280 nm optical density ratio and Bioanalyzer 2100 (Agilent, Santa Clara, CA) prior to transcriptome analyses. Microarray experiments were performed using Affymetrix (Santa Clara, CA) Human U133 Plus 2.0 GeneChip by the Laboratory of Molecular Technology, Frederick National Laboratory for Cancer Research, Frederick, MD, USA. cRNA probe synthesis, hybridization, and scanning of arrays followed the manufacturers' default protocols. Probe signal values and detection calls were determined using Affymetrix GeneChip Command and Console Software. Chip-to-Chip variations were normalized by the Robust Multichip Average normalization algorithm.

Multivariate analysis. GeneChip data were exported to BRB-ArrayTools, an open source microarray statistical analysis plug-in for the Microsoft Excel software (Microsoft Professional 2003). The non-supervised hierarchical clustering approach was chosen for the data set exploration.

Class comparison analysis. The class comparison module in BRB-ArrayTools was utilized to identify differentially and statistically significantly expressed genes between sample groups. Microarray data from different comparison pairs were subjected to a two-sample t-test (with random variance model). Type I error correction was applied to all pairwise comparisons. Pairwise analysis was performed using control vs. treated using a fold cut-off of > 3.

Pathway analysis. Gene lists winnowed from the multivariate analyses were exported to the Ingenuity Pathway Analysis (IPA) web portal (http://www.ingenuity.com) for functional pathway analysis.

Statistical analysis

All experiments were performed at least three times, each time at least in triplicate. Results are presented as averages ± SE. Statistical tests of chemical and protein results were carried out using GraphPad Instat version 3.00 (GraphPad Software, San Diego, CA). Pairwise comparisons included the t test, with the Welch correction or application of the Mann–Whitney test as appropriate. Significance of correlations was assessed by the Pearson linear correlation or the Spearman test as appropriate.

Results

GSH-dependent dearylation is a major metabolic pathway for JS-K in the cell

Cellular redox potential is largely controlled by GSH, which accounts for more than 90% of cellular non-protein thiols [7]. JS-K was designed to release NO upon nucleophilic attack by free thiols (particularly GSH). The first step in the metabolism of JS-K in the cell is the dearylation of the diazeniumdiolate by GSH via a nucleophilic aromatic substitution reaction, liberating the ionic diazeniumdiolate moiety CEP/NO, which spontaneously hydrolyzes, releasing NO (Fig. 1). Subsequent oxidation products of the NO can react with additional equivalents of GSH. A consequence of this metabolism is a rapid depletion of cellular GSH concurrent with a rise in oxidized glutathione (GSSG) (Fig. 1).

JS-K is relatively stable in complete (RPMI 1640, 10% FBS) cell culture medium, with a half-life of about 5 h. However, it is rapidly and completely metabolized by the cells. Liquid chromatography/mass spectrometry (LC/MS) analysis revealed that 30 min after addition of JS-K to the cell culture the parent compound is not detectable in the lysate; we have found glutathione and cysteine adducts derived from JS-K (Fig. 2), the latter presumably resulting from further metabolism of the glutathione conjugate. The parent compound was also not detected after shorter treatment (10 min); however, in this case only the glutathione adduct was seen (data not shown).

JS-K has a major impact on cellular redox status

We quantified GSH and GSSG levels in the U937 leukemia cell line, which grows in suspension as spherical cells. As described under Materials and Methods, we determined the average cell volume to be 4.0 ± 0.5 pL, and measured total amounts of GSH and GSSG. Concentrations per cell and the reduction potential of the GSH redox couple were calculated. Table 1 shows changes in cellular GSH/GSSG concentrations and reduction potential in U937 leukemia cells after JS-K treatment. One-hour treatment with JS-K led to a decrease in total GSH concentration, a decrease in GSH/GSSG ratio, and a rise in reduction potential.

A noteworthy feature of the data in Table 1 is the extent to which low concentrations of JS-K in the medium can generate major changes in cellular GSH/GSSG levels. For example, 1 µM JS-K in the medium dropped the intracellular GSH level by 730 µM, while 4 µM JS-K consumed 1970 µM GSH and increased GSSG by 110 µM. Although the depletion of hundreds of micromoles of GSH by low µM concentrations of JS-K may seem counter-intuitive, a closer look at the stoichiometry provides a rationale. Assuming that the number of moles of JS-K is equally dispersed amongst the cells in suspension, 1.5 fmol and 6 fmol are delivered per cell when JS-K is added to the medium at 1 µM and 4 µM concentrations, respectively. Upon metabolism and NO production, a significant portion of the 13.7 fmol of GSH per cell is consumed, 2.9 fmol from 1 µM treatment and 7.9 fmol from 4 µM treatment, translating to an observable decrease in the cellular GSH concentration.

U937 cells were pretreated with N-acetylcysteine (NAC), a precursor for GSH synthesis and a nucleophilic reducing agent, to determine whether it attenuates the disruption of redox balance. Indeed, pretreatment with NAC prevented the depletion of GSH

Table 1
Alterations in cellular redox potential.

NAC	Treatment	GSH (mM)	GSSG (mM)	Redox potential (mV)	ΔE (mV)
None	DMSO	3.43 ± 0.14	0.20 ± 0.01	− 227.6	
	JS-K 1 µM	2.70 ± 0.16	0.21 ± 0.01	− 219.1	
	JS-K 4 µM	1.46 ± 0.16	0.31 ± 0.02	− 197.7	29.9
0.1 mM	DMSO	4.30 ± 0.15	0.18 ± 0.01	− 233.8	
	JS-K 1 mM	3.75 ± 0.23	0.24 ± 0.01	− 227.2	
	JS-K 4 µM	2.55 ± 0.22	0.37 ± 0.04	− 209.8	24.0
1 mM	DMSO	6.74 ± 0.18	0.16 ± 0.01	− 247.6	
	JS-K 1 µM	6.01 ± 0.26	0.18 ± 0.01	− 243.6	
	JS-K 4 µM	5.40 ± 0.26	0.25 ± 0.02	− 236.8	10.8

associated with JS-K treatment alone and partially prevented the rise in reduction potential (Table 1). Time-dependent study revealed that the rise in reduction potential was significant within minutes of treatment with 1 µM JS-K (Fig. 3), consistent with rapid reaction of the prodrug with GSH. We have shown previously that the rate of reaction with GSH is important for anticancer efficacy of aryl-diazeniumdiolate-based NO-releasing prodrugs [17,19].

Depletion of cellular antioxidant defenses allows for the generation of significant quantities of ROS, which have been suggested to induce apoptosis [16]. The release of NO from JS-K in the cells was confirmed by DAF fluorescence assay (Fig. 4(A)). There was also an increase in DCFH-DA-reactive material, suggesting an increase in oxidizing equivalents. One-hour treatment with 0.5 µM JS-K resulted in an increase in DCF fluorescence, which was more pronounced at higher concentrations of the prodrug (Fig. 4(B)). It may be noted that DCFH-DA reacts with reactive nitrogen species such as peroxynitrite ([10,13]).

Oxidative stress leads to activation of cellular stress signaling and apoptosis

Oxidative stress is widely observed to activate the stress kinases p38 and SAPK/JNK pathways, leading to activation of stress-response genes. Phosphorylation of p38 was very rapidly

induced by JS-K. A strong signal was observed as soon as 5 min after treatment with JS-K was initiated and it continued for several hours; at the 16-h time point the signal was significantly reduced (Fig. 5(A)). Importantly, pretreatment with NAC encumbered phosphorylation of p38, suggesting that redox imbalance/oxidative stress is a triggering mechanism in this pathway's activation (Fig. 5(B)). Phosphorylation of the p38 downstream target ATF2 exhibited the same pattern. SAPK/JNK activation was detected slightly later, about 1 h after JS-K treatment was initiated. Phosphorylation of its downstream target, transcription factor c-jun, was observed after 1 h as well.

We have shown previously that upregulation of activating transcription factor 3 (ATF3) is required for cell killing by aryl-diazeniumdiolate-based NO-releasing prodrugs in non-small cell lung cancer (NSCLC) cells [17]. Here we observed a significant increase in ATF3 protein in the leukemia cells as well, starting 4 h after JS-K treatment was initiated.

To determine whether the induction of ROS/RNS and stress signaling was associated with cell death, cells were treated with JS-K and then analyzed by Western blot for markers of apoptosis. Apoptosis was activated early, initially through the extrinsic pathway, as evidenced by caspase-8 activation within 2 h of treatment with 1 µM JS-K (Fig. 6(A)). Cleaved effector caspase-7 and cleaved PARP signals were also observed within 2 h (Fig. 6(A)).
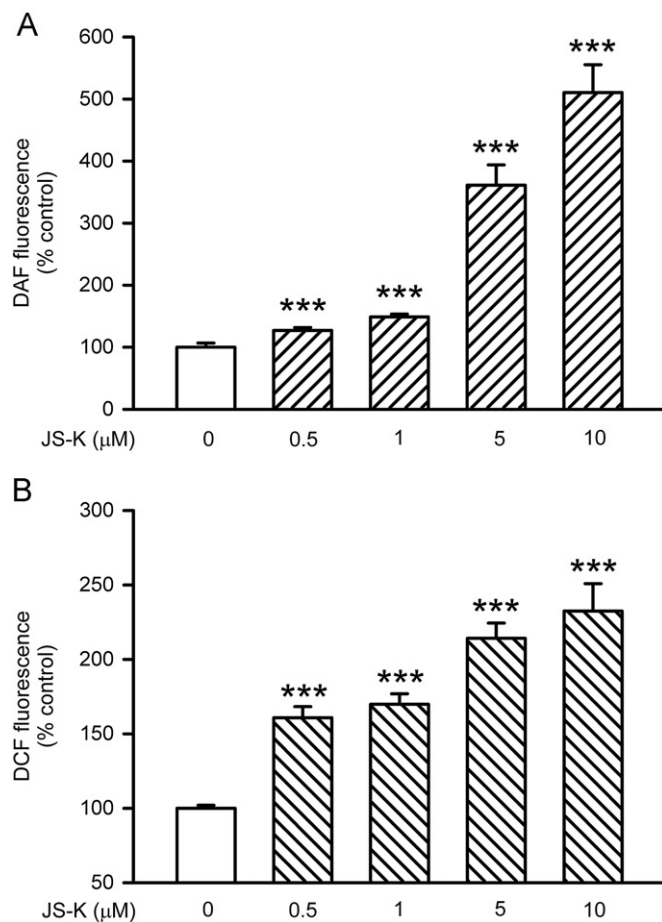
JS-K-induced U937 cell death is blocked by NAC

As shown in Table 1, pretreatment with NAC increased the basal levels of GSH, and diminished the rise in reduction potential. Moreover, NAC blocked JS-K-induced U937 cell apoptosis (Fig. 6(B)). U937 cells (5×10^5/mL) were pretreated with 0.1 or 1 mM NAC for 16 h, followed by 3 h with 1 µM JS-K. Pretreatment with NAC inhibited activation of apoptosis, as evidenced by diminished cleavage of caspases-8 and -3.

Loss of mitochondrial membrane potential after JS-K treatment

Fig. 7(A) shows loss of mitochondrial membrane potential in U937 cells after 4 h incubation with 1 µM JS-K; there was even more significant loss of this membrane potential with 5 µM JS-K (Fig. 7(A)). A similar effect of JS-K was observed previously in H1703 NSCLC cells after 1 h of incubation with 1 µM drug [17]. One-hour treatment did not result in loss of mitochondrial membrane potential in U937 cells, suggesting that the sequence of events could be cell-type specific, and that in U937 cells apoptosis by an extrinsic pathway precedes involvement of mitochondria in the cell death pathway. Collapse of mitochondrial membrane potential has been shown to represent a stage of cell death that is already irreversible [32]. Mitochondrial apoptosis was also activated, as evidenced by presence of cytochrome *c* in cytosol after 4 h treatment with JS-K (Fig. 7(B)).

Microarray analysis

To provide an assessment of transcripts and pathways altered by JS-K, treated cells were subjected to microarray analysis. Treatment with JS-K resulted in differential expression of 1800 transcripts, suggesting an extensive response to JS-K. Marked upregulation of expression of JUN and ATF3 (Table 2) confirms the protein results shown in Fig. 5 and indicates regulation of these at the mRNA level. The c-MYC oncogene was downregulated progressively with time (Table 2). We confirmed downregulation of the protein level of this short-lived transcription factor by Western blot. As shown in Fig. 8(B), c-myc protein expression

Fig. 4. (A) Intracellular NO release in U937 cells after JS-K treatment measured as DAF fluorescence. (B) Intracellular ROS/RNS level after JS-K treatment measured as DCF fluorescence. Cells were loaded with the probe for 30 min, followed by 1-h treatment with JS-K at concentrations indicated on the graph. A representative experiment is shown ($n=6$). ***$P < 0.0001$, by two-tailed paired *t* test, compared with cells treated with DMSO only.
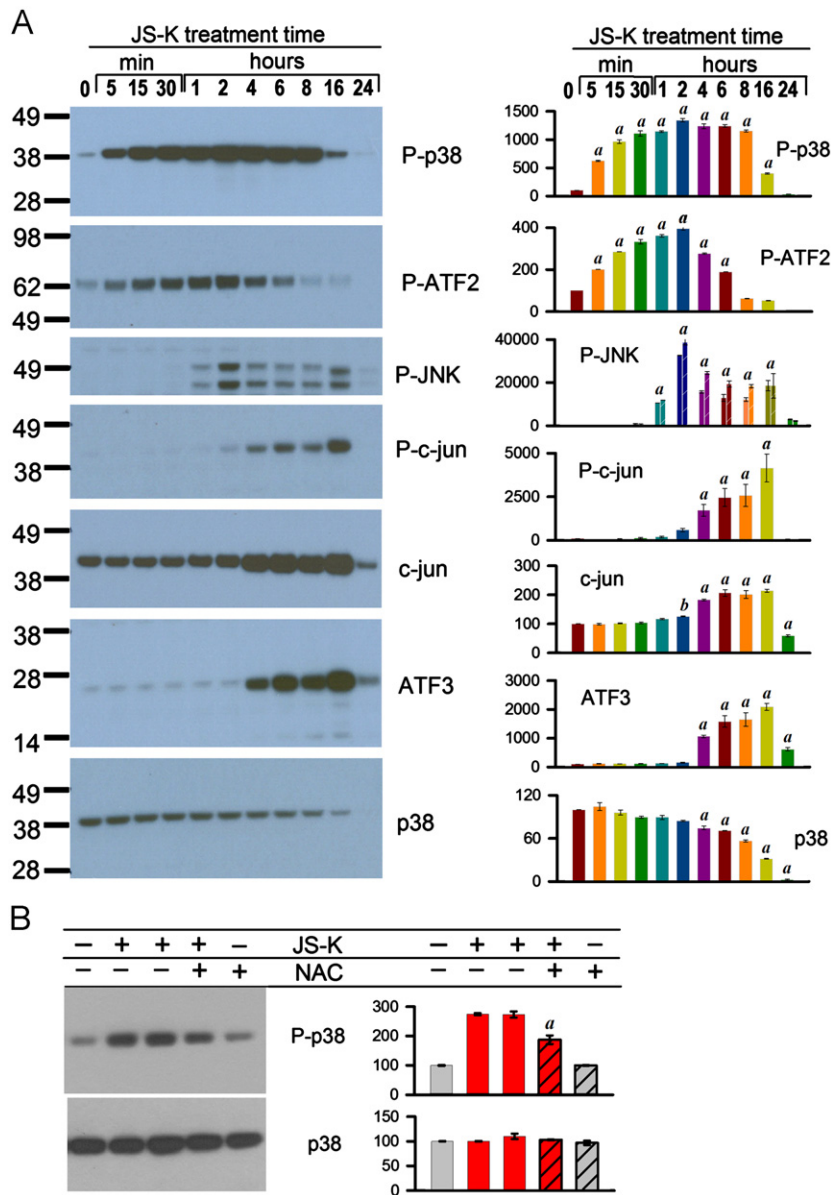
Fig. 5. Activation of stress signaling pathways in U937 cells after JS-K treatment. (A) JS-K very rapidly induced phosphorylation of p38 and its downstream target ATF2. Phosphorylation of SAPK/JNK and its downstream target c-jun, as well as upregulation of c-jun protein level, were observed later, after 1-h treatment with the drug. Significant upregulation of ATF3 protein level occurs after 4 h with the drug. Representative Western blots (left panel), and percentage of control (at zero time point) quantitative densitometric values (mean ± SD) from 2 or 3 independent experiments (right panel) are shown. a $P < 0.001$; b $P < 0.01$, compared to time zero. (B) Pretreatment with 1 mM NAC for 16 h prevented p38 phosphorylation after 30 min treatment with 1 μM JS-K. Representative Western blot (left panel) and percentage of untreated control densitometric values (mean ± SD from 3 independent experiments) (right panel) are shown. Phosphorylation of p38 was significantly reduced by pretreatment with NAC (a $P < 0.001$, by two-tailed paired t test, compared with cells treated with JS-K).

was downregulated rapidly, with complete loss of signal after 2 h of treatment with JS-K.

As expected, the transcriptome from treated cells was enriched in genes implicated in the response to oxidative stress. NF-E2-related factor 2 (NFE2L2, Nrf2) is considered as one of the major transcription factors activated in response to oxidative stress. Upon oxidative stress Nrf2 translocates to the nucleus and upon heterodimerization with other transcription factors (e.g., JunD, ATF4, small MAFs) transactivates the anti-oxidant response elements of many cytoprotective genes, as well as Nrf2 itself. In our study, NFE2L2 transcript was upregulated 1.4-, 1.6-, and 5-fold at 1.5, 4 and 24 h, respectively. Similarly, JunD was upregulated 1.8-, 4.8-, and 3-fold at the same time points. Expression of many Nrf2-regulated genes

was altered. NQO1 (NADPH: quinone oxidoreductase 1), a major detoxification enzyme, was upregulated 2, 2.6 and 4-fold, at 1.5, 4 and 24 h, respectively. Antioxidant HMOX1 (heme oxygenase 1) was upregulated 5-fold at 1.5 h and 31-fold at 4 h, then its transcript level decreased. Transcript of the rate-limiting enzyme in glutathione synthesis, GCLM (glutamate-cysteine ligase, modifier subunit) was upregulated 2-fold at 1.5 h and 4-fold at 4 h. Similarly, SLC7A11, a cystine/glutamate antiporter, was upregulated over 2-fold at 1.5 h and over 7-fold at 4 h. These changes appear to be triggered by depletion of GSH from the cell in a cellular attempt to restore its supply.

Complete microarray data have been deposited on the GEO website http://www.ncbi.nlm.nih.gov/geo (GEO Accession number GSE42344).
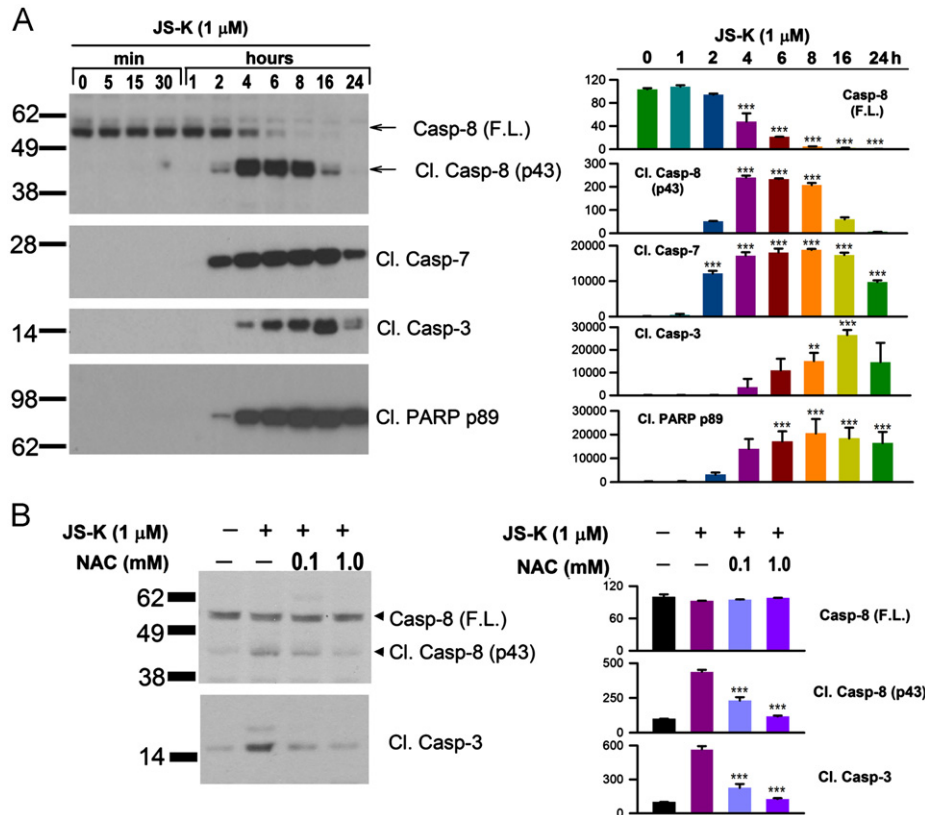
Fig. 6. Treatment with JS-K induced the extrinsic apoptosis pathway in U937 cells. (A) Cleavage of caspase-8 and the effector caspase-7, as well as PARP, was seen within 2 h after addition of the drug. Representative Western blots (left panel), and percentage of control (at zero time point) quantitative densitometric values (mean ± SD) from 2 or 3 independent experiments (right panel) are shown. F.L. – full length caspase. *** $P < 0.001$, compared to 0-h control. (B) Pretreatment with NAC (0.1 or 1 mM) for 16 h encumbered activation of apoptosis. Cleaved caspase-8 and -3 signals are significantly diminished in cells pretreated with NAC. Representative Western blots (left panel) and percentage of untreated control quantitative densitometric values (mean ± SD, right panel) are shown; F.L.—full length caspase 8; Cl.—cleaved fragment (43 kDa); *** $P < 0.001$, compared to JS-K-treated cells.
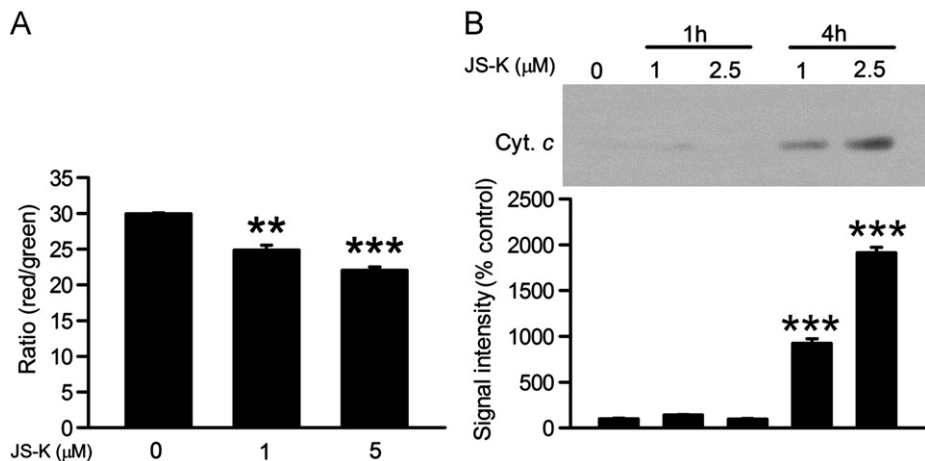

Fig. 7. Treatment with JS-K induced the intrinsic apoptosis pathway in U937 cells. (A) Mitochondrial membrane potential (ΔΨm) was analyzed using JC-1 mitochondrial membrane dye. U937 cells were treated with DMSO (control) or JS-K (1 or 5 μM) for 4 h. The drug caused an increase in the green (JC-1 monomers) and decrease in the red fluorescence (JC-1 aggregates) indicative of loss of ΔΨm. Ratio of JC-1 (red to green) was calculated. **$P < 0.001$, ***$P < 0.0001$, by two-tailed paired t-test, compared to control cells, treated with DMSO. (B) Cytochrome c release to cytosol was observed 4 h after JS-K treatment. Representative Western blot and percentage of control quantitative densitometric values (mean ± SD) are shown. ***$P < 0.0001$, by two-tailed paired t-test, compared to control cells, treated with DMSO.

Discussion

Oxidative stress occurs when there is an imbalance between the rates of ROS generation and removal by scavenging mechanisms. Glutathione is a ubiquitous cellular thiol. Its reduced form (GSH) and oxidized form (GSSG) constitute the major thiol redox system in cells, and proper GSH/GSSG redox balance is crucial for cell function.

Activation of the nitric oxide-releasing prodrug JS-K to release NO through nucleophilic aromatic substitution depletes cells of

Table 2
Most significant alterations in gene expression after JS-K treatment.

Gene symbol	Description	Fold change		
		90 min	4 h	24 h
Genes most upregulated				
IL8	Interleukin 8	38.73	82.10	39.46
JUN	Jun oncogene	26.40	17.73	14.42
TRIB1	Tribbles homolog 1 (Drosophila)	15.84	36.92	35.84
PRDM1	PR domain containing 1, with ZNF domain	15.06	11.81	15.23
MMP1	Matrix metallopeptidase 1 (interstitial collagenase)	13.06	12.03	100.96
MAFB	v-maf Musculoaponeurotic fibrosarcoma oncogene homolog B (avian)	12.81	22.96	46.63
FZD7	Frizzled homolog 7 (Drosophila)	11.02	9.37	6.11
EGR3	Early growth response 3	10.52	5.09	1.49
FOS	v-fos FBJ murine osteosarcoma viral oncogene homolog	9.78	2.34	2.15
ATF3	Activating transcription factor 3	9.35	15.24	31.36
FABP4	Fatty acid binding protein 4, adipocyte	8.20	8.36	28.29
MXD1	MAX dimerization protein 1	7.21	6.81	3.83
KLF6	Kruppel-like factor 6	6.65	7.44	8.05
EMP1	Epithelial membrane protein 1	5.52	20.24	305.46
FOXO3	Forkhead box O3	5.46	3.18	2.04
HMOX1	Heme oxygenase (decycling) 1	5.30	31.54	3.40
C5AR1	Complement component 5a receptor 1	5.04	21.11	116.57
IER3	Immediate early response 3	3.93	14.05	71.61
PALLD	Palladin, cytoskeletal associated protein	1.09	11.10	22.60
CDKN1A	Cyclin-dependent kinase inhibitor 1A (p21, Cip1)	2.83	10.68	46.40
TREM1	Triggering receptor expressed on myeloid cells 1	3.59	10.04	49.94
ADFP	Adipose differentiation-related protein	4.26	9.96	9.03
FPR1	Formyl peptide receptor 1	2.14	9.34	55.67
GPR34	G protein-coupled receptor 34	1.72	1.83	60.34
TDO2	Tryptophan 2,3-dioxygenase	1.05	1.15	46.91
CREB5	cAMP responsive element binding protein 5	1.05	3.21	44.56
CCL3	Chemokine (C-C motif) ligand 3	1.02	8.96	41.19
PHLDA1	Pleckstrin homology-like domain, family A, member 1	1.85	5.22	35.93
TRIB1	Tribbles homolog 1 (Drosophila)	15.84	36.92	35.84
CD86	CD86 molecule	1.01	1.03	26.48
Genes most downregulated				
ACSM3	Acyl-CoA synthetase medium-chain family member 3	−7.33	−7.76	−7.92
FDFT1	Farnesyl-diphosphate farnesyltransferase 1	−6.38	−6.79	−7.04
SCD	Stearoyl-CoA desaturase (delta-9-desaturase)	−6.09	−9.73	−6.17
SC4MOL	Sterol-C4-methyl oxidase-like	−6.01	−10.93	−4.10
INSIG1	Insulin induced gene 1	−5.60	−7.86	−5.00
SNRPN	Small nuclear ribonucleoprotein polypeptide N	−5.27	−5.30	−5.13
ACSS2	Acyl-CoA synthetase short-chain family member 2	−4.73	−3.46	−2.26
GSTA4	Glutathione S-transferase A4	−4.36	−3.28	−3.06
MARS2	Methionyl-tRNA synthetase 2, mitochondrial	−1.08	−12.24	−24.75
HMGCS1	3-Hydroxy-3-methylglutaryl-Coenzyme A synthase 1 (soluble)	−4.30	−12.16	−7.13
DPP7	Dipeptidyl-peptidase 7	−3.96	−8.04	−12.50
PTCD2	Pentatricopeptide repeat domain 2	−2.33	−7.49	−7.83
POLR1B	Polymerase (RNA) I polypeptide B, 128 kDa	−1.08	−7.43	−13.86
MYC	v-myc Myelocytomatosis viral oncogene homolog (avian)	−2.79	−6.88	−19.79
POLR1B	Polymerase (RNA) I polypeptide B, 128 kDa	−1.08	−7.43	−13.86

GSH, and increases ROS, which causes further oxidation of GSH and formation of GSSG. We have for the first time quantified loss of GSH and increase in GSSG as a function of treatment of cancer cells with an arylated diazeniumdiolate prodrug. Our results demonstrate that depletion of the cellular glutathione pool is an important first step in the cytotoxic action of JS-K. Thanks to the rapid and complete uptake of the micromolar levels of JS-K from the culture medium, it was on scale to effectively impact milli-molar concentrations of GSH in the cell. Depletion of GSH as a therapeutic strategy in sensitizing cancer cells to radiation therapy has been demonstrated [8]. Cancer cells depleted of GSH through inhibition of its synthesis with buthionine sulfoximine (BSO) were much more sensitive to the effects of irradiation.

It will be noted that JS-K is a particularly efficient consumer of GSH, with each molecule imported into the cell being capable of destroying multiple reducing species through GSH-arylation and oxidation of NO to form reactive nitrogen species (Fig. 1). That such significant consumption of GSH by JS-K was indeed

operative in these cells was confirmed in our experiments. As stated in the Results, the number of moles of JS-K delivered per cell is in the same scale as the number of moles of GSH. Each mole of JS-K irreversibly arylates a mole of GSH, resulting in release of two moles of NO, the oxidation products of which are capable of consuming more reduced equivalents of GSH (Fig. 1). This con-sumption of GSH results in a rise in the steady-state level of ROS/RNS, further consuming GSH, with a concurrent increase in GSSG (Table 1). Additional ROS likely are produced as a result of the damage to cellular catalytic systems (e.g., mitochondria), and this ROS causes further depletion of GSH, an additional 6 fmol of GSH per cell from a 24 h treatment with1 μM JS-K. Export of GSSG from the cell may also contribute to depletion of cellular GSH and rise in reduction potential, as GSSG is a known endogenous substrate for multidrug resistance proteins [3].

SAPK/JNK and p38 stress kinases are important mediators of cell death signaling resulting from a variety of cellular stresses, including ROS/RNS. We have reported previously that SAPK/JNK
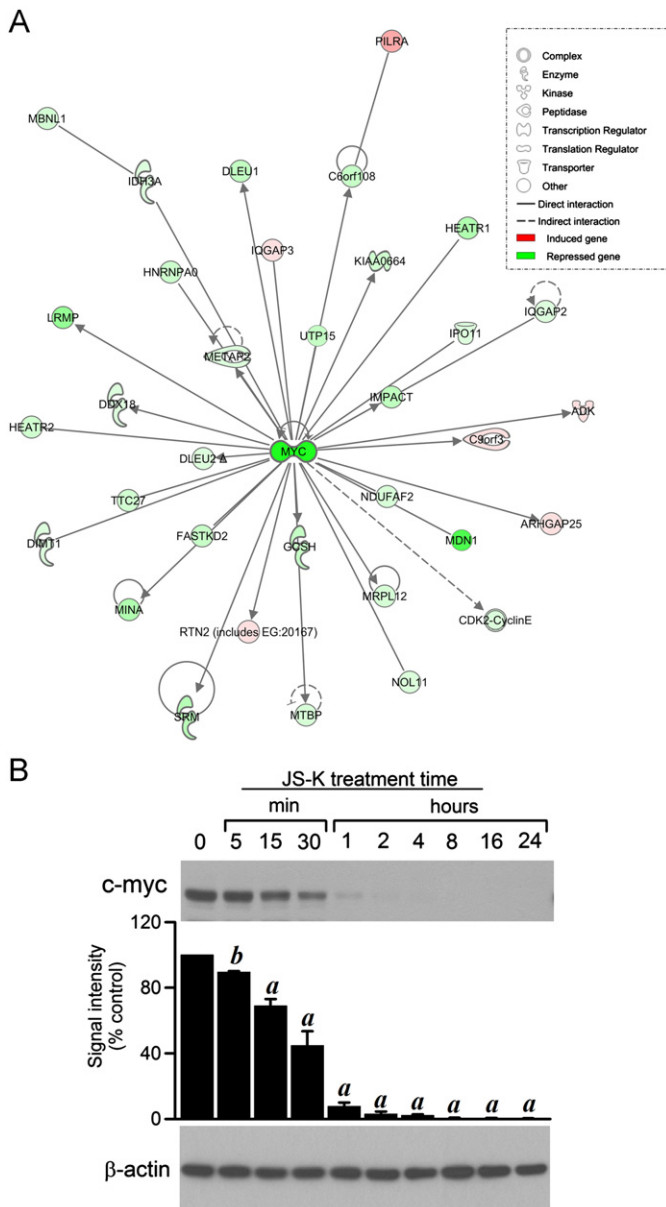
Fig. 8. JS-K inhibited c-myc oncogene expression in U937 cells. (A) Downregulation of MYC-dependent transcripts after JS-K treatment. Based upon the Ingenuity Knowledge Database, IPA pathway analysis revealed an interactive gene network around MYC. The network indicated that MYC is upstream of many important genes and may play a critical role in different pathways. Data processed for IPA analysis were based upon the differentially and statistically significant expressed gene set at the 24-h time point. (B) Downregulation of c-myc protein expression after JS-K treatment. Representative blot and percentage of control quantitative densitometric values (mean $\pm$ SD) are shown. a, $P < 0.001$; b, $P < 0.01$, compared to 0-h control cells. Actin serves as a loading control.

activation is a consequence of JS-K treatment in NSCLC cells *in vitro* and in xenografts [17]. Involvement of the SAPK/JNK pathway in activation of apoptotic cell death has been reported [30], as well as its involvement in ATF3 induction [4]. Kiziltepe and colleagues have shown that activation of SAPK/JNK in multiple myeloma cells in response to JS-K is a critical step in the apoptotic pathway's activation, and that pretreatment with JNK inhibitor II rescued multiple myeloma cells from apoptosis.

In leukemia U937 cells, however, we observed rapid activation of p38, preceding SAPK/JNK phosphorylation. Phosphorylation and activation of p38 by peroxynitrite have been reported in neuroblastoma cells [21]. Decrease in p38 phosphorylation upon

JS-K treatment has been noted in breast cancer cells [28]. The involvement of ROS in JS-K activity was further illustrated by experiments showing that the reducing agent NAC protected against p38 activation and apoptotic cell death.

Microarray analysis provided some useful additional information about this leukemia cell model. Increases in c-jun and ATF3 protein were preceded by changes in gene expression. A number of genes presented marked up- or down-regulation. These included cancer-related genes such as *MAF* and *FOS* oncogenes that could be targeted for combination therapy along with JS-K. Similarly, several antioxidant factors were upregulated, which, if individually targeted, could increase the effectiveness of JS-K even further.

Progressive and marked downregulation of the proto-oncogene c-*MYC* revealed by microarray, and confirmed by immunoblot, is especially notable, in view of its frequent involvement in hematopoietic cancers. In various lymphomas and leukemias it inhibits differentiation and functions as a leukemogenic protein. C-*MYC* gene amplification and translocation, resulting in its deregulation, have been observed in Burkitt's lymphoma and acute lymphoblastic leukemia ([6]; [2]). Inactivation of the *MYC* oncogene has also been shown sufficient to induce regression of invasive liver cancers [25].

In summary, we have shown that in U937 leukemia cells a micromolar concentration of the NO-donor prodrug JS-K is sufficient to induce major depletion in GSH, due to its rapid, complete uptake from the culture media and subsequent cascade of reactions with NO-derived species. Marked progressive increase in cellular ROS/RNS and change in cellular reduction potential result, followed by cellular stress signaling, downregulation of c-myc, and initiation of apoptosis. This mechanistic information may be useful for enhancement of the efficacy of JS-K and similar drugs.

Acknowledgments

References

[1] M.E. Anderson, Determination of glutathione and glutathione disulfide in biological samples, Methods in Enzymology 113 (1985) 548–555.

[2] A. Ar-Rushdi, K. Nishikura, J. Erikson, R. Watt, G. Rovera, C.M. Croce, Differential expression of the translocated and the untranslocated c-myc oncogene in Burkitt lymphoma, Science 222 (1983) 390–393.

[3] N. Ballatori, S.M. Krance, R. Marchan, C.L. Hammond, Plasma membrane glutathione transporters and their roles in cell physiology and pathophysiology, Molecular Aspects of Medicine 30 (2009) 13–28.

[4] Y. Cai, C. Zhang, T. Nawa, T. Aso, M. Tanaka, S. Oshiro, et al., Homocysteine-responsive ATF3 gene expression in human vascular endothelial cells: activation of c-Jun NH2-terminal kinase and promoter response element, Blood 96 (2000) 2140–2148.

[5] H. Chakrapani, R.C. Kalathur, A.E. Maciag, M.L. Citro, X. Ji, L.K. Keefer, et al., Synthesis, mechanistic studies, and anti-proliferative activity of glutathione/glutathione S-transferase-activated nitric oxide prodrugs, Bioorganic and Medicinal Chemistry 16 (2008) 9764–9771.

[6] R. Dalla-Favera, M. Bregni, J. Erikson, D. Patterson, R.C. Gallo, C.M. Croce, Human c-myc oncogene is located on the region of chromosome 8 that is translocated in Burkitt lymphoma cells, Proceedings of the National Academy of Sciences of the United States of America 79 (1982) 7824–7827.

[7] S.M. Deneke, B.L. Fanburg, Regulation of cellular glutathione, American Journal of Physiology 257 (1989) L163–L173.

[8] J.K. Dethmers, A. Meister, Glutathione export by human lymphoid cells: depletion of glutathione by inhibition of its synthesis decreases export and increases sensitivity to irradiation, Proceedings of the National Academy of Sciences of the United States of America 78 (1981) 7492–7496.

[9] O.W. Griffith, Determination of glutathione and glutathione disulfide using glutathione reductase and 2-vinylpyridine, Analytical Biochemistry 106 (1980) 207–212.

[10] B. Halliwell, M. Whiteman, Measuring reactive species and oxidative damage in vivo and in cell culture: how should you do it and what do the results mean? British journal of Pharmacology 142 (2004) 231–255.

[11] B. Halliwell, Oxidative stress and cancer: have we moved forward? Biochemical Journal 401 (2007) 1–11.

[12] D.P. Jones, Redox potential of GSH/GSSG couple: assay and biological significance, Methods in Enzymology 348 (2002) 93–112.

[13] B. Kalyanaraman, V. Darley-Usmar, K.J. Davies, P.A. Dennery, H.J. Forman, M.B. Grisham, et al., Measuring reactive oxygen and nitrogen species with fluorescent probes: challenges and limitations, Free Radical Biology and Medicine 52 (2012) 1–6.

[14] A.S. Kamiguti, L. Serrander, K. Lin, R.J. Harris, J.C. Cawley, D.J. Allsup, et al., Expression and activity of NOX5 in the circulating malignant B cells of hairy cell leukemia, Journal of Immunology 175 (2005) 8424–8430.

[15] T. Kiziltepe, T. Hideshima, K. Ishitsuka, E.M. Ocio, N. Raje, L. Catley, et al., JS-K, a GST-activated nitric oxide generator, induces DNA double-strand breaks, activates DNA damage response pathways, and induces apoptosis in vitro and in vivo in human multiple myeloma cells, Blood 110 (2007) 709–718.

[16] C. Langer, J.M. Jürgensmeier, G. Bauer, Reactive oxygen species act at both TGF-beta-dependent and -independent steps during induction of apoptosis of transformed cells by normal cells, Experimental Cell Research 222 (1996) 117–124.

[17] (a) A.E. Maciag, H. Chakrapani, J.E. Saavedra, N.L. Morris, R.J. Holland, K.M. Kosak, et al., The nitric oxide prodrug JS-K is effective against non-small-cell lung cancer cells in vitro and in vivo: involvement of reactive oxygen species, Journal of Pharmacology and Experimental Therapeutics 336 (2011) 313–320;
(b) A.E. Maciag, R.S. Nandurdikar, S.Y. Hong, H. Chakrapani, B. Diwan, N.L. Morris, et al., Activation of the c-Jun N-terminal kinase/activating transcription factor 3 (ATF3) pathway characterizes effective arylated diazeniumdiolate-based nitric oxide-releasing anticancer prodrugs, Journal of Medicinal Chemistry 54 (2011) 7751–7758.

[18] V. McMurtry, J.E. Saavedra, R. Nieves-Alicea, A.M. Simeone, L.K. Keefer, A.M. Tari, JS-K, a nitric oxide-releasing prodrug, induces breast cancer cell death while sparing normal mammary epithelial cells, International Journal of Oncology 38 (2011) 963–971.

[19] R.S. Nandurdikar, A.E. Maciag, R.J. Holland, Z. Cao, P.J. Shami, L.M. Anderson, et al., Structural modifications modulate stability of glutathione-activated arylated diazeniumdiolate prodrugs, Bioorganic and Medicinal Chemistry 20 (2012) 3094–3099.

[20] V. Nogueira, Y. Park, C.C. Chen, P.Z. Xu, M.L. Chen, I. Tonic, et al., Akt determines replicative senescence and oxidative or oncogenic premature senescence and sensitizes cells to oxidative apoptosis, Cancer Cell 14 (2008) 458–470.

[21] K. Oh-Hashi, W. Maruyama, K. Isobe, Peroxynitrite induces GADD34, 45, and 153 VIA p38 MAPK in human neuroblastoma SH-SY5Y cells, Free Radical Biology and Medicine 30 (2001) 213–221.

[22] Z. Ren, S. Kar, Z. Wang, M. Wang, J.E. Saavedra, B.I. Carr, JS-K, a novel non-ionic diazeniumdiolate derivative, inhibits Hep 3B hepatoma cell growth and induces c-Jun phosphorylation via multiple MAP kinase pathways, Journal of Cellular Physiology 197 (2003) 426–434.

[23] J.E. Saavedra, A. Srinivasan, C.L. Bonifant, J. Chu, A.P. Shanklin, J.L. Flippen-Anderson, et al., The secondary amine/nitric oxide complex ion $R_2N[N(O)NO]^-$ as nucleophile and leaving group in S_NAr reactions, Journal of Organic Chemistry 66 (2001) 3090–3098.

[24] A.A. Sablina, A.V. Budanov, G.V. Ilyinskaya, L.S. Agapova, J.E. Kravchenko, P.M. Chumakov, The antioxidant function of the p53 tumor suppressor, Nature Medicine 11 (2005) 1306–1313.

[25] C.M. Shachaf, A.M. Kopelman, C. Arvanitis, A. Karlsson, S. Beer, S. Mandl, et al., MYC inactivation uncovers pluripotent differentiation and tumour dormancy in hepatocellular cancer, Nature 431 (2004) 1112–1117.

[26] P.J. Shami, J.E. Saavedra, L.Y. Wang, C.L. Bonifant, B.A. Diwan, S.V. Singh, et al., JS-K, a glutathione/glutathione S-transferase-activated nitric oxide donor of the diazeniumdiolate class with potent antineoplastic activity, Molecular Cancer Therapeutics 2 (2003) 409–417.

[27] P.J. Shami, J.E. Saavedra, C.L. Bonifant, J. Chu, V. Udupi, S. Malaviya, et al., Antitumor activity of JS-K [O^2-(2,4-dinitrophenyl) 1-[(4-ethoxycarbonyl)pi-perazin-1-yl]diazen-1-ium-1,2-diolate] and related O^2-aryl diazeniumdio-lates in vitro and in vivo, Journal of Medicinal Chemistry 49 (2006) 4356–4366.

[28] A.M. Simeone, V. McMurtry, R. Nieves-Alicea, J.E. Saavedra, L.K. Keefer, M.M. Johnson, et al., TIMP-2 mediates the anti-invasive effects of the nitric oxide-releasing prodrug JS-K in breast cancer cells, Breast Cancer Research 10 (2008) R44.

[29] C. Sundström, K. Nilsson, Establishment and characterization of a human histiocytic lymphoma cell line (U-937), International Journal of Cancer 17 (1976) 565–577.

[30] C. Tournier, P. Hess, D.D. Yang, J. Xu, T.K. Turner, A. Nimnual, et al., Requirement of JNK for stress-induced activation of the cytochrome c-mediated death pathway, Science 288 (2000) 870–874.

[31] A. Weyerbrock, N. Osterberg, N. Psarras, B. Baumer, E. Kogias, A. Werres, et al., JS-K, a glutathione S-transferase-activated nitric oxide donor with antineo-plastic activity in malignant gliomas, Neurosurgery 70 (2012) 497–510.

[32] N. Zamzami, P. Marchetti, M. Castedo, C. Zanin, J.L. Vayssière, P.X. Petit, et al., Reduction in mitochondrial potential constitutes an early irreversible step of programmed lymphocyte death in vivo, Journal of Experimental Medicine 181 (1995) 1661–1672.

[33] Y. Zhou, E.O. Hileman, W. Plunkett, M.J. Keating, P. Huang, Free radical stress in chronic lymphocytic leukemia cells and its role in cellular sensitivity to ROS-generating anticancer agents, Blood 101 (2003) 4098–4104.